Impact of Soil Structure on Microwave Volume Scattering Evaluated by a Two-Dimensional Numerical Model

Charles Onier, André Chanzy, André Chambarel, Raphaël Rouveure, Myriam Chanet, and Hervé Bolvin

***Abstract*—Soil volumetric structure is an important parameter for tillage operation. The aim of this paper is to assess whether volume characteristics can be inferred from radar measurements. A 2-D numerical model (the 2DSCAT model) was developed based on a numerical solver using a time-domain finite-element method to solve Maxwell's equations. Perfectly matched layers were implemented as well as a near- to far-field transformation. A focused incident beam was generated by adapting the boundary conditions. To represent the soil structure, a simulator was developed describing the soil as biphasic media (fine earth and clods). Clods were represented by randomly deformed ellipses, with randomly determined dimensions, locations, and orientations. The model performed successfully, as evaluated against exact analytical solutions available for an infinite perfectly conducting cylinder and the reflection of flat semi-infinite media. The model was then evaluated against measurements made by an X-band FM continuous-wave radar on a box filled with dry clods of different sizes. The effect of the clod size on the backscattering power was very well reproduced, showing the potential of using a 2-D numerical model to understand microwave-backscattering patterns from cloddy soils. Analysis of the volume scattering shows that this phenomenon can be mostly hidden in the scatter diagram by surface scattering when the latter occurred. However, the volume scattering gives a stronger residual signal in time because of propagation through the medium. Thus, time studies of the scattering signal provide further information about volume heterogeneities.**

Manuscript received October 5, 2009; revised April 26, 2010; accepted June 13, 2010. Date of publication July 26, 2010; date of current version December 27, 2010.

C. Onier was with the Unité Mixte de Recherche "Environnement Méditerranéen et Modélisation des AgroHydrosytème, Institut National de la Recherche Agronomique et Université d'Avignon et des Pays de Vaucluse (UMR EMMAH, INRA/UAPV), 84914 Avignon Cédex 9, France. He is now with the Laboratoire d'Electronique Antennes et Télécommunications, Nice-Sophia Antipolis University, France (e-mail: ch.onier@gmail.com).

A. Chanzy is with the Unité Mixte de Recherche "Environnement Méditerranéen et Modélisation des AgroHydrosytème, Institut National de la Recherche Agronomique et Université d'Avignon et des Pays de Vaucluse (UMR EMMAH, INRA/UAPV), 84914 Avignon Cédex 9, France (e-mail: achanzy@avignon.inra.fr).

A. Chambarel, retired, was with the Unité Mixte de Recherche "Environnement Méditerranéen et Modélisation des AgroHydrosytème, Université d'Avignon et des Pays de Vaucluse et Institut National de la Recherche Agronomique (UMR EMMAH, UAPV/INRA), 84914 Avignon Cédex 9, France.

R. Rouveure and M. Chanet are with the Unité de Recherche de Technologie des Systèmes d'Information pour les Agrosystèmes, Centre d'Etude du Machinisme Agricole et du Génie Rural des Eaux et Forêts (CEMAGREF), 63172 Aubière Cédex, France.

H. Bolvin is with the Unité Mixte de Recherche "Environnement Méditerranéen et Modélisation des AgroHydrosytème, Université d'Avignon et des Pays de Vaucluse et Institut National de la Recherche Agronomique (UMR EMMAH, UAPV/INRA), 84914 Avignon Cédex 9, France.

Color versions of one or more of the figures in this paper are available online at http://ieeexplore.ieee.org.

Digital Object Identifier 10.1109/TGRS.2010.2053714

***Index Terms*—Agricultural practices, microwave, numerical modeling, radar remote sensing, soil structure, surface roughness, tilled soil, volume scattering.**

I. Introduction

VOLUME-SCATTERING signals may provide remote and nondestructive information regarding the inner structure of a heterogeneous medium. In this paper, we tested whether microwave-scattering measurements made by a radar installed at the back of a tractor could be used to characterize clod size after a tillage operation. This is an important agronomic parameter that needs to be assessed in order to appreciate the quality of seedbed preparation [1]. Beyond this practical question lies a more fundamental question of the role of soil 3-D structure in the scattering processes.

Microwave volume scattering is often advanced as an explanation for the disagreement between radar or radiometer measurements and soil microwave emission or backscattering models that, in most cases, consider only surface scattering. However, a few studies have quantified or modeled soil volume scattering, particularly that induced by soil clods, which fall within the size of the wavelength range. Theoretically, microwaves penetrate soil through the top layers. This was observed by the measured reflection from a metal plate inserted below the soil surface [2] or the detection of subsurface geological discontinuities [3]. Moreover, [2] suggested the existence of volume scattering since the extinction coefficient had to be increased in order to model the soil emission when a metal plate was inserted into the soil. Using a theoretical analysis, [4] showed that disklike inclusions significantly affected backscattering coefficients. However, the size of the inclusion ($\sim$in millimeters) and the dielectric-constant contrast with the matrix (> 70) were not representative of soil-structure patterns.

Most of the models used to retrieve soil moisture from microwave measurements describe the surface scattering as the Integral Equation Model (IEM) model [5]. Numerous studies were devoted to the evaluation of such models using references from either numerical simulations [6], [7] or measurements made under well-controlled conditions. [8], [9]. Comparisons are, in general, satisfactory with reasonable errors (1–3 dB with the scattered signal or 0.1 with the soil emissivity). Surface-scattering models were revealed to be very sensitive to soil roughness characterization [10], which is very difficult to obtain at the scale of the microwave measurements [11]. Therefore, it is not easy to isolate from model/experience comparisons the

volume contribution to the total scattering. An implicit way to account for volume scattering in surface-scattering models has been to play on the depth of the layer used to characterize soil moisture. However, surface-scattering models sometimes failed in simulating backscattering measurements over the range of moisture conditions and angular configurations, particularly with cloddy soil [12], when a single depth was used to simulate all conditions and configurations. Accounting for moisture gradients near the surface to compute the soil reflectivity led to a difference that is lower than 1 dB [13], [14], which could not explain the observation/simulation discrepancies. Therefore, the microwave scatter patterns may change when soil dries, explaining why surface-roughness parameter has been found to vary with soil moisture [15]. A recent study [16] has shown a strong interaction between the moisture sampling depth and the roughness parameters, demonstrating that the soil volume-scattering component may lead to a compromise for soil moisture and roughness characterization. Schneeberger *et al.* [17] proposed an original approach to represent topsoil structure, but their model does not distinguish the roles of surface roughness and soil structure. To our knowledge, a clear evaluation of surface and volume-scattering contributions to the total scattering from structured soil has never been shown.

To evaluate such contributions, experimental analyses are not appropriate since the total scattering can only be measured. An alternative method is provided by numerical models that solve Maxwell's equations in heterogeneous media by considering the heterogeneity geometry explicitly. A wide choice of computational methods exists [18]. For our objective, time-domain approaches, as used in the time-domain finite-element method (FEM) (TDFEM) or the finite-difference time-domain (FDTD) method, are preferred since they can easily give results in the time and frequency domain using a Fourier transform. In our study, we adopted the TDFEM approach. It provides stability and precision while offering great flexibility in the partitioning of domains, exhibiting a complex geometry and the possibility of introducing boundary conditions of various natures [19]. The TDFEM allows 1-, 2-, and 3-D representations. A 3-D approach is necessary to represent the wave scattering from heterogeneous media as soils. However, to represent domains that are large enough to smooth speckle effects and meshes that are fine enough to represent soil structure geometry, very large meshes are necessary. A 2-D approach is then an alternative (the number of meshes can be divided by more than 100) to have a numerical problem of reasonable size. However, the 2-D representation implies that the heterogeneities have an infinite extension along the direction perpendicular to the modeled plan and prevents the representation of depolarization. Using the FDTD method, simulations of the scattering patterns from an ellipsoid and a cylinder, which present similar cross sections, have led to different scattered electromagnetic (EM) fields [20] showing, in this case, the limit of a 2-D approach. However, the authors have also shown that the scattering EM field from a parallelepiped having similar cross section is much more different than the other two targets. These differences were established from isolated canonic targets, and conclusions can be different with complex 3-D media. To represent such media and to have a reasonable computation time, we adopted, in this paper, a 2-D approach and evaluated it by comparing simulated results with experimental measurements made on targets having a well-controlled 3-D structure.

Freshly tilled soil can be considered as a biphasic medium with clod embedded in fine earth. Both phases differ by their dielectric constant due to the difference in soil moisture and dry bulk density. The surface is defined as the resultant of the soil fine-earth roughness and the clod position near the surface, which are more or less inserted in the soil. To compute the representative scattering patterns of a given target, numerous simulations are required to smooth the variability induced by the spatial arrangement of the reflectors within the computation domain. For every simulation, independent descriptions of the soil structure are needed to establish an explicit permittivity map. Such maps are very difficult to measure and are generated by a soil-structure model.

In this paper, we present a 2-D scattering simulator (hereafter referred to as 2DSCAT) that represents microwave-scattering measurement of a medium as agricultural soil. It contains a solver based on a TDFEM model developed to simulate time-domain reflectometry measurements. Boundary conditions were adapted to produce a Gaussian beam, and a near-field to far-field transformation (NFFT) was implemented to compute the scattering diagrams. Perfectly matched layers (PMLs) were introduced at the edge of the computation domain in order to represent an open area by a finite domain. The solver is combined with a soil-structure generator, based on an aggregate approach recently used in soil science for seedbed description [21], in order to control the size of the clods. The solver was first validated against analytical solutions. Then, its ability to represent microwave scattering from heterogeneous media composed of aggregates was established using experimental data. Finally, the impact of aggregates embedded in a soil matrix on the scattering signal was assessed.

II. Theory

A. Formulation of Maxwell's Equations and Numerical Resolution

To solve the Maxwell's equations with the FEM, rotational equations for the electric field and the magnetic field were written in a dimensionless form

$$[\mu_r]\frac{\partial \mathbf{H}}{\partial t} = -\nabla \times \mathbf{E} - Re \cdot [\sigma_r^*]\,\mathbf{H} \tag{1}$$

$$[\varepsilon_r]\frac{\partial \mathbf{E}}{\partial t} = \nabla \times \mathbf{H} - Rm \cdot [\sigma_r]\mathbf{E} \tag{2}$$

where μ_r is the relative magnetic permeability, ε_r is the relative permittivity, σ_r is the relative electric conductivity, and σ_r^* is a fictive magnetic conductivity, which is necessary to introduce absorbing layers. $\mathbf{H}$ and $\mathbf{E}$ are the dimensionless electric and magnetic fields, the components of which were divided by H_0 and E_0 being linked by

$$H_0 = E_0 \cdot \sqrt{\frac{\varepsilon_0}{\mu_0}}. \tag{3}$$

Distances are divided by a characteristic length l, and time is divided by the characteristic time $\tau = l/c$, where c is the wave velocity in the void. The dimensionless equations introduced two dimensionless terms

$$Rm = \sigma_0 \cdot \mu_0 \cdot l \cdot c \tag{4}$$

$$Re = \sigma_0^* \cdot \varepsilon_0 \cdot l \cdot c \tag{5}$$

where σ_0 and σ_0^* are reference electric conductivity and fictive magnetic conductivity, respectively.

Equations (1) and (2) can be integrated over the spatial domain (Ω) and its boundary (Γ) and rewritten in a weak formulation using the Galerkin weighting ($\delta\mathbf{H}$ and $\delta\mathbf{E}$). Following the transformations proposed by [22], we obtained, for the transverse-electric (TE) mode

$$\int_{(\Omega)} \delta\mathbf{H} \cdot [\mu_r] \frac{\partial \mathbf{H}}{\partial t} \cdot d\Omega = -\int_{(\Omega)} \delta\mathbf{H} \cdot (\nabla \times \mathbf{E}) \cdot d\Omega - \int_{(\Omega)} \delta\mathbf{H} \cdot Re \cdot [\sigma_r^*]\, \mathbf{H} \cdot d\Omega \tag{6}$$

$$\int_{(\Omega)} \delta\mathbf{E} \cdot [\varepsilon_r] \frac{\partial \mathbf{E}}{\partial t} \cdot d\Omega = \int_{(\Omega)} \mathbf{H} \cdot (\nabla \times \delta\mathbf{E}) \cdot d\Omega - \int_{(\Gamma)} (\delta\mathbf{E} \wedge \mathbf{H}) \hat{\mathbf{n}} \cdot d\Gamma - \int_{(\Omega)} \delta\mathbf{E} \cdot Rm \cdot [\sigma_r]\mathbf{E} \cdot d\Omega. \tag{7}$$

Similar equations can be obtained for the transverse-magnetic mode. Since we limited our study to the TE mode, we do not present the equations for the other modes. In (6) and (7), the boundary conditions can be easily introduced in the integral term over (Γ). To solve (6) and (7), we used a C++ object-oriented programming for the finite-element code called fast adaptive finite-element modular object (FAFEMO) [22], [23].

B. Boundary Conditions

Due to the weak formulation with the natural boundary conditions and the Huygens principle, we only have to enter the incident field at the edge of the computation domain as a function of time and location. Considering an incident wave having an incident angle θ, we can define the Cartesian references $(\mathrm{S}\mathbf{XY})$, where $\mathbf{X}$ is the unit vector along the propagation direction, and $\mathbf{Y}$ is perpendicular to it. The field value at point $\mathrm{M}(XY)$ of the boundary can be written as

$$E(M,t) = F(X,t) \cdot g(Y) \tag{8}$$

where $F(X,t)$ defines the pulse shape in time and $g(Y)$ defines its shape in space. A Rayleigh-shaped pulse was implemented

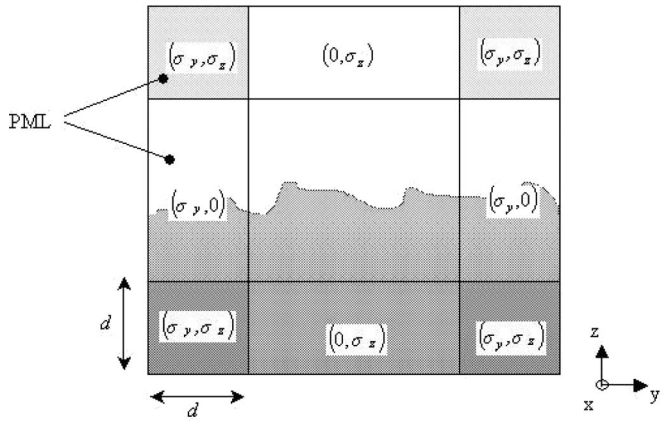

Fig. 1. σ_y and σ_z in the computation domain. d is the thickness of the PML.

for $F(X,t)$, which covered a range of frequencies

$$F(X,t) = \text{Real}\left(j \Big/ \left(\left(2\pi f\left(t - \frac{X}{c}\right)\Big/ 4\right) + j\right)^5\right). \tag{9}$$

where f is the central frequency having the maximum energy.

A 2-D Gaussian intensity beam $g(Y)$ was obtained according to the following:

$$g(Y) = e^{(-\alpha \cdot Y^2)} \tag{10}$$

with α representing a parameter function of the width of the spot. This allowed simulating a focused beam, as generated by most antennas, and focusing the energy in the middle of the computation domain to limit edge effects.

C. Absorbing Layer

Absorbing layers were set at the edge of the computation domain (Fig. 1) to limit its size and reduce parasitic reflections. We chose the Berenger PML technique, which led to satisfactory results [24], [25]. Around the computational domain, as shown in Fig. 1, we implement the following equations given for the 2-D case and the TE mode with the EM components (E_x, H_y, H_z) [26]

$$\varepsilon \cdot \frac{\partial E_{xy}}{\partial t} + \sigma_y \cdot E_{xy} = \frac{\partial H_z}{\partial y} \tag{11}$$

$$\varepsilon \cdot \frac{\partial E_{xz}}{\partial t} + \sigma_z \cdot E_{xz} = -\frac{\partial H_y}{\partial z} \tag{12}$$

$$\mu \cdot \frac{\partial H_y}{\partial t} + \sigma_z^* \cdot H_y = -\frac{\partial}{\partial z}(E_{xy} + E_{xz}) \tag{13}$$

$$\mu \cdot \frac{\partial H_z}{\partial t} + \sigma_y^* \cdot H_z = \frac{\partial}{\partial y}(E_{xy} + E_{xz}) \tag{14}$$

with $E_x = E_{xy} + E_{xz}$. No reflection occurs at the boundary between the propagation media and the PML when $\sigma_y/\varepsilon = \sigma_y^*/\mu$ if the boundary is perpendicular to the y-axis, and $\sigma_z/\varepsilon = \sigma_z^*/\mu$ if the boundary is perpendicular to the z-axis.

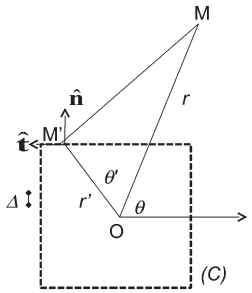

Fig. 2. Geometry of the NFFT problem.

In the PML proposed by Berenger, σ increases gradually in relation with the wave penetration in the PML according to

$$\sigma(z) = \left(\frac{z}{d}\right)^m \cdot \sigma_{\max} \tag{15}$$

with

$$\sigma_{\max} = -\frac{(m+1)\ln[R(0)]}{2\eta d} \tag{16}$$

where $\eta = (\mu/\varepsilon)^{1/2}$, $R(0)$ is the normal reflection coefficient, d is the total PML thickness, and m is the polynomial order; z is the depth of the PML with respect to its inner border.

These values were chosen by considering the residual reflection of a plane wave by the PML with a normal incidence. We optimized m and $R(0)$ for a PML thickness set to $d = 0.105$ m. With $m = 3$ and $R(0) = 10^{-5}$, the ratio of the reflected energy to the incident energy was equal to -98 dB.

D. NFFT

Due to the equivalence principle, we can calculate the far fields from the near fields recorded on a contour (C) for the 2-D case (Fig. 2). We implemented an NFFT formula derived from the Stratton–Chu formula in the frequency domain using $e^{-j\omega t}$ convention [25], [27]–[29]. For every point $M(x, r, \theta)$ defined in a cylindrical coordinate system $(O, \hat{\mathbf{x}}, \hat{\mathbf{r}}, \hat{\theta})$, the EM field $(\mathbf{E}, \mathbf{H})$ is given from to the field $(\mathbf{E}', \mathbf{H}')$ on (C) by

$$\mathbf{E}(M,\omega) = \int_{(C)} [j\omega\mu G(\hat{\mathbf{n}} \times \mathbf{H}') + (\hat{\mathbf{n}} \cdot \mathbf{E}')\nabla' G + (\hat{\mathbf{n}} \times \mathbf{E}') \times \nabla' G]\, dl' \tag{17}$$

$$\mathbf{H}(M,\omega) = \int_{(C)} [-j\omega\varepsilon G(\hat{\mathbf{n}} \times \mathbf{E}') + (\hat{\mathbf{n}} \cdot \mathbf{H}')\nabla' G + (\hat{\mathbf{n}} \times \mathbf{H}') \times \nabla' G]\, dl' \tag{18}$$

with G as the Green function and $\hat{\mathbf{n}}$ as the normal vector to (C) in the 2-D plan at the integration point $M'(r', \theta')$.

In the TE case, with the EM components (Ex, Hr, H_θ) and the far-field approximation

$$G = \frac{j}{4} H_0^{(1)}(k|r - r'|) \tag{19}$$

with k as the wavenumber and $H_0^{(1)}$ as the zero-order Hankel function of the first kind, which can be approximated when $r \gg r'$ by

$$H_0^{(1)}(k|r - r'|) \approx \sqrt{\frac{2}{j\pi kr}} e^{jkr} e^{-jkr' \cos(\theta' - \theta)}. \tag{20}$$

With the time expressed in the propagation equation as $e^{-j\omega t}$

$$\nabla' G \approx -jkG\hat{\mathbf{r}}. \tag{21}$$

As E' is perpendicular to the plan including C, (17) can be simplified considering that

$$(\hat{\mathbf{n}} \cdot \mathbf{E}')\nabla' G = \mathbf{0}. \tag{22}$$

Similarly, $\hat{\mathbf{n}} \times \mathbf{H}'$ is along the $\hat{\mathbf{x}}$ direction, and so it can be written as

$$(\hat{\mathbf{n}} \times \mathbf{H}') = (\hat{\mathbf{n}} \times \mathbf{H}')_x \cdot \hat{\mathbf{x}}. \tag{23}$$

The tangential vector to (C) in the 2-D plan at the integration point M' is defined by $\hat{\mathbf{t}}$. Therefore, we can write $\hat{\mathbf{t}} \times \hat{\mathbf{r}} = -(\hat{\mathbf{t}} \cdot \hat{\boldsymbol{\theta}}) \cdot \hat{\mathbf{x}}$, and the approximation made in (21) is expressed by

$$\begin{aligned}(\hat{\mathbf{n}} \times \mathbf{E}') \times \nabla' G &\approx (\hat{\mathbf{n}} \times \mathbf{E}')_t \hat{\mathbf{t}} \times (-jkG)\hat{\mathbf{r}} \\ &\approx j\omega\varepsilon\eta(\hat{\mathbf{n}} \times \mathbf{E}')_t(\hat{\mathbf{t}} \cdot \hat{\boldsymbol{\theta}})G\hat{\mathbf{x}}.\end{aligned} \tag{24}$$

For a discrete contour with n points and a step of Δ, the Ex field can be finally derived from (17) and (19)–(24) as follows:

$$\begin{aligned}E_x(M,\omega) \approx \frac{\omega}{4}\sqrt{\frac{2}{jk\pi}}\frac{e^{jkr}}{\sqrt{r}} \cdot \Bigg[&-\mu \sum_{i=1}^{n} (\hat{\mathbf{n}} \times \mathbf{H}')_x e^{-jkr' \cos(\theta' - \theta)} \Delta \\ &- \varepsilon\eta \sum_{i=1}^{n} (\hat{\mathbf{t}} \cdot \hat{\boldsymbol{\theta}})(\hat{\mathbf{n}} \times \mathbf{E}')_t e^{-jkr' \cos(\theta' - \theta)} \Delta \Bigg].\end{aligned} \tag{25}$$

Equation (25) is defined for a closed contour. For an open contour, a correction term should be added. However, we can still calculate a good approximation of the EM field without this term [27], and the correction is generally omitted. The results can be plotted in polar coordinates to give a scattering diagram. $\mathbf{E}'$ and $\mathbf{H}'$ in (25) are obtained by a Fourier transformation of the field over time and are computed for every point by the solver.

E. Numerical Characteristics

Simulations were performed in TE mode using a Rayleigh pulse with a central frequency of 3 GHz. The size of the simulated domain was 0.9 by 0.3 m. The domain was meshed using regular triangles with the size set to $\lambda/50$ (λ being the wavelength), and so, 750 000 elements were necessary to cover the calculation domain. Elementary properties were determined from the soil map considering that the element properties

Fig. 3. Soil representation simulated by the soil-geometry simulator. The fine earth is in gray, and clods are in black.

corresponded to the element's center of gravity. Note that no refinement was performed in the vicinity of the surface (clod, soil). The time step corresponds to 1 ps, and the simulated time was 2.85 ns. The NFFT was performed with an open contour, which was a straight horizontal line over the target. To minimize computation time, the FAFEMO solver was parallelized, and an expert system was implemented to restrict the computation domain to the portion already crossed by the EM wave.

F. Soil-Geometry Simulator

We model the heterogeneities found in tilled soils. In fact, we assume that tilled soil can be represented by two phase media with clods of different sizes embedded in a continuous medium which corresponds to fine earth (Fig. 3). Both phases are assumed to have distinct dielectric constant since the clods are more compact than fine earth, thus leading to different levels of volumetric water content. The soil-generator principle is then to include in a homogeneous medium having a rough upper boundary (the fine earth), random-shaped entities (the clods), the characteristics of which can be defined and controlled separately. In this paper, we represented clods by ellipses, with randomly deformed contours to reproduce clod-surface irregularities. The soil-geometry simulation was done according to the following phases.

1) The proportions of clods and fine earth were defined. According to the clod-size distribution law, we drew a set of ellipse sizes until we reached a cumulative surface that corresponded to the proportion of clods. In this study, the ratio between the small and the great axis of the ellipses was kept constant.
2) A random surface was generated for the fine-earth phase, considering Gaussian and exponential autocorrelation functions.
3) For every clod, a deformation was calculated by adding a random difference to the ellipse radius. This was made for every directions sampled with a 1° increment. From the computed new radii, a spline function was used to close the clod boundary. In this study, the random difference was drawn using a Gaussian law and a standard deviation of $0.09 \cdot r$ (r being the radius).
4) Clods were then successively positioned within the domain. The location of the center of every clod and the orientation of its great axis were randomly determined within given limits. The overlapping with already positioned clods was computed. If it was greater than a prescribed percentage, a new random location was drawn.

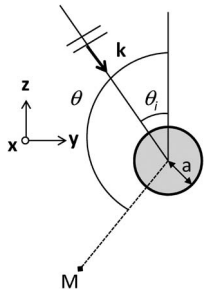

Fig. 4. Geometry of the infinite-cylinder problem. $\mathbf{k}$ is the incident wave vector, θ_i is the incidence angle, a is the cylinder radius, and $M(r, \theta)$ is the watching point.

The soil-geometry simulator was therefore based on the following main parameters:

1) proportion of aggregates with respect to fine earth in the medium;
2) mean and standard deviation of the clod-size distribution, the maximum overlapping threshold, and the distribution law to compute ellipse deformation;
3) ellipse-orientation distribution and deformation statistics;
4) distribution characteristics (standard deviation of the heights, correlation length, and autocorrelation function) of the fine-earth surface profile.

An example of a soil representation computed by the soil-geometry simulator is given in Fig. 3.

The simulated soil geometry is then taken to allocate to every element the EM properties of their center of gravity.

III. Validation of the 2DSCAT Model on Exact Solution

A. Analytical Solution to Validate the EM Model

In order to validate the 2DSCAT model, tests were performed on two simple targets: an infinite perfectly conducting cylinder and a homogeneous semi-infinite medium with a planar surface. For the infinite perfect conductor, we took the exact solution for the scattered EM fields [30]. In the 2-D case with a cylindrical coordinate $(O, \hat{\mathbf{x}}, \hat{\mathbf{r}}, \hat{\boldsymbol{\theta}})$, as shown in Fig. 4, we considered an incident plane wave field $\mathbf{E}_x^i$ of incidence θ_i and wavenumber k, given by

$$\mathbf{E}_i^x(r, \theta) = \sum_{n=-\infty}^{+\infty} j^n e^{-jn\theta_i} J_n(kr) e^{jn\theta}. \tag{26}$$

The fields scattered by a cylinder of radius a can then be written as follows:

$$\mathbf{E}_x^s(r, \theta) = \sum_{n=-\infty}^{+\infty} \left(-\frac{J_n(ka)}{H_n^{(1)}(ka)} \right) \cdot H_n^{(1)}(kr) e^{jn\theta} \cdot j^n e^{-jn\theta_i} \tag{27}$$

where J_n and $H_n^{(1)}$ are the Bessel and the Hankel function of the first kind.

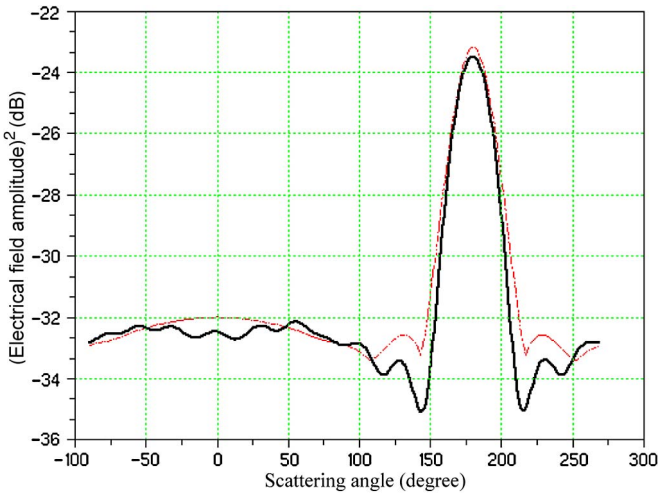

Fig. 5. Far-field scattering diagram from a perfectly conducting infinite cylinder having a diameter of 1.4λ. Bold line is simulated with the 2DSCAT model and the dash-dot curve corresponds to the analytical solution [(26) and (27)].

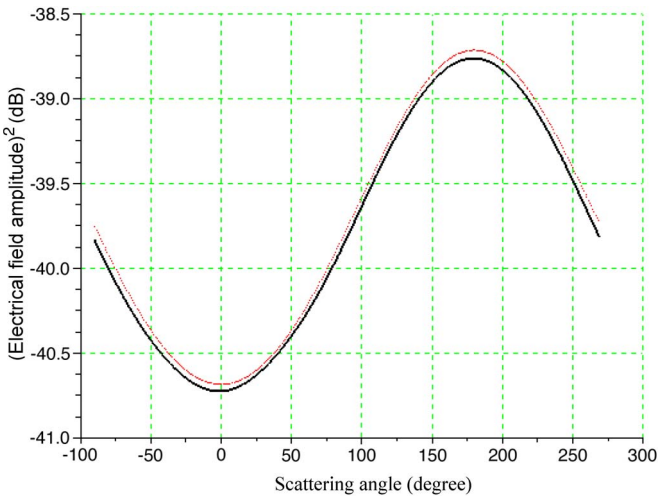

Fig. 6. Same as Fig. 5, with a cylinder diameter of 0.1λ.

Using (27), we computed the scatter diagrams for two diameter sizes (0.1λ and 1.4λ) and compared these diagrams with those given by the EM model.

For the reflection of a homogeneous semi-infinite medium with a planar surface, we compared the reflection coefficient for different permittivities (5, 10, 15, and 20) and incidence angles (10°, 30°, and 50°). The theoretical reflection coefficient is given by the Fresnel formula. The simulated reflection coefficients were computed with the NFFT, using, as a contour line, a straight line located just above the media.

For these simulations, the incident EM field was a plane wave pulse.

B. Results

The scattering diagrams in Figs. 5 and 6 show the results for a perfectly conducting cylinder with a diameter of 1.4λ and 0.1λ, respectively. Simulations made by the 2DSCAT model respect the shape of the scattering diagram and the magnitude of the scattering field from perfectly conducting cylinders having

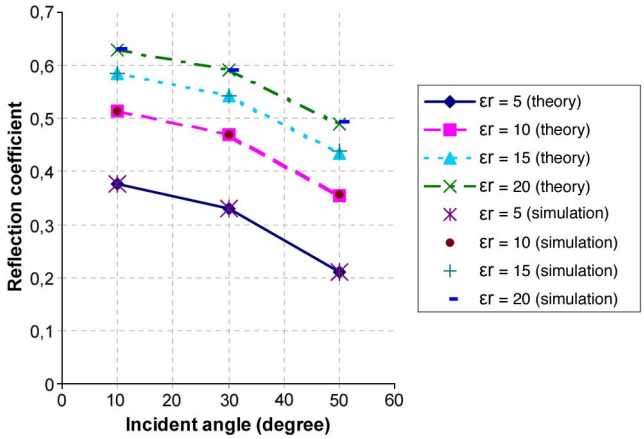

Fig. 7. Theoretical and simulated reflection coefficients as a function of the incidence angle for a homogeneous semi-infinite flat medium.

contrasting diameters. In the case of a small cylinder, the mesh was refined around it, and the square contour used to implement the NFFT was set very close to the cylinder (0.05λ). The simulated fluctuations ($\sim$1 dB) observed in Fig. 5 with the large cylinder were induced by the location of the NFFT contour, which was too far from the cylinder (0.5λ). Such a result stresses the importance of having the NFFT contour near the scattering target.

Fig. 7 shows the reflection coefficients for a homogeneous semi-infinite medium with plane surface at different incidence angles. We can see that all the simulated reflected fields are in very good agreement with the theoretical values, even for the large incidence angle of 50°.

The successful comparison of the 2DSCAT model with the exact analytical solutions shows that the numerical method is well implemented and that the numerical parameters are adequate. Moreover, this validates the NFFT, which was calculated with an open contour.

IV. Evaluation of the 2DSCAT Model on Experimental Measurements

A. Experiments

We verified that the 2DSCAT model simulated the influence of soil structure by making measurements under controlled conditions. The experimental data were collected using an FM continuous-wave radar operating at 10 GHz and HH polarization [31]. Measurements were made in an anechoic chamber. Backscattering power measurements were made on a box filled with dry soil clods, which could be handled easily as they had a good mechanical stability. Moreover, dry condition was a favorable condition to obtain a homogeneous dielectric permittivity within and between clods. Power measurements were normalized by that measured on a horizontal metal plate. Measurements were performed at nadir on different targets that differed by the clod-size classes: 5–6.3, 6.3–10, 10–12.5, 12.5–16, 16–20, 20–25, and 25–31 mm. For a given aggregate-size class, 50 replications were done. For each replication, the box was emptied and refilled with the same aggregates, and a characterization of the surface roughness was determined. Soil

TABLE I
SOIL CHARACTERISTICS FOR LABORATORY EXPERIMENTS

Clods size normalized by the wavelength	Height rms normalized by the wavelength
0.188	0.027
0.272	0.053
0.375	0.080
0.475	0.117
0.600	0.157
0.750	0.197
0.933	0.260

Fig. 8. Example of the aggregate-box representation given by the soil-structure generator.

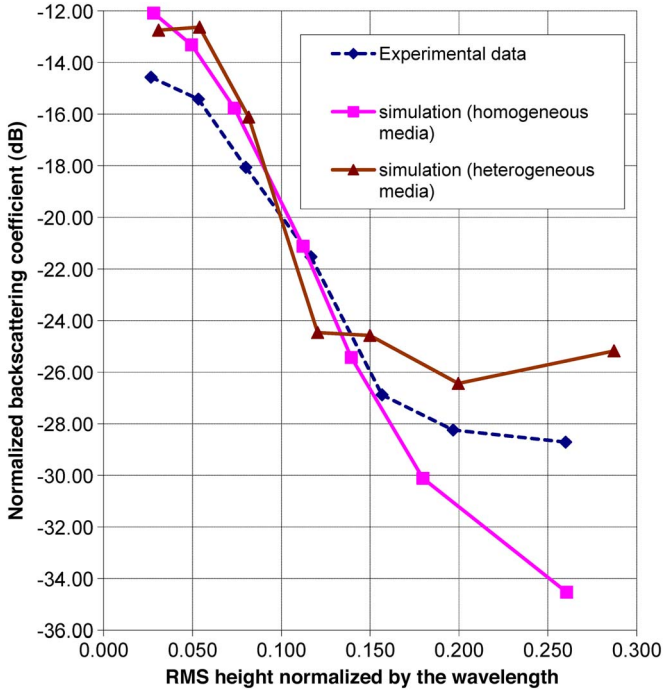

Fig. 9. Experimental and the simulated backscattering power measurements, normalized by power reflection on a horizontal metal plate, as a function of the surface rms height normalized by the wavelength. The homogeneous medium has a random rough boundary according to an exponential distribution law.

characteristics are displayed in Table I. Then, radar measurements were averaged and normalized by the center wavelength.

To reproduce this experiment, we generated a batch of 30 permittivity maps for each clod-size class using the soil-geometry simulator. The heterogeneous medium (Fig. 8) was supposed to be an air–clod mix, the clod having a relative permittivity of three, which corresponds to a very dry soil. Moreover, the soil maps were selected in order to filter those having a roughness similar to the experimental case. A simulation with a metal plate was also performed to normalize the simulated backscattering power, as done with the experimental results. All simulations were conducted with nadir angle of incidence. Normalized backscattering coefficients from 30 replications were then averaged and compared with the averaged experimental results.

To address the impact of soil structure, a homogeneous medium was simulated with $\varepsilon_r = 3$, and a surface profile was generated using an exponential autocorrelation function. Thirty replications were simulated, and the normalized backscattering power was averaged.

B. Results

Fig. 9 shows the normalized backscattering measurements for the different clod-size classes. The experimental data are about 2.5 dB below the simulations. This may be explained by an error of the reflected-power measurement from the metal plate whose horizontality is difficult to obtain, an error on the determination of the dielectric constant, and/or the representation of the soil media. Nevertheless, the 2DSCAT simulator is able to simulate backscattering power variations according to the clod size. The unexpected low value for the $H_{\rm rms}$ case of 0.12λ corresponds to an aggregate size of $\lambda/2$. Such a drop may be explained by the rise of destructive interactions due to the elliptical shape of the aggregates and their particular size with respect to the wavelength. These two points were different in the experimental conditions since the aggregate size was not unique, and the shape of the aggregates might be more complex.

The results also show differences between homogeneous and heterogeneous media when the clod size is large. This can be explained by the impact of volume scattering due to soil-structure heterogeneities and/or by the ability of an exponential autocorrelation function to describe the surface roughness of cloddy soils investigated in this study.

The comparison with experimental results shows that the combination of the 2DSCAT model and the soil-geometry model leads to a relevant description of microwave-scattering patterns of heterogeneous media, with aggregates having a size comparable with the wavelength. This result strengthens the relevance of using 2-D modeling to represent the microwave scattering from complex tilled soil. Without making specific simulations in 2-D and 3-D configurations, it is difficult to assess the error made by a 2-D modeling. However, our results show that the 3-D processes have little impact on the copolarized backscattered power from a complex target with many scatterers.

V. ANALYSIS OF THE SCATTERING PROCESSES FROM TILLED BARE SOILS

We studied the impact of the volume scattering of soil-like media. For this, we considered two media: one having a flat surface and clods embedded in the soil (case 1) and

TABLE II
SOIL CHARACTERISTICS FOR TILLED SOIL

Simulation Case	Case 1	Case 2
Surface roughness Hrms (mm)	0	6.7
Clod sizes	$\lambda/5$	$\lambda/5$ to $\lambda/2$
Clod proportion in the medium	51%	26%
Relative permittivity of clods	10	8.5
Relative permittivity of fine earth	5	6
Relative permittivity of the homogeneous equivalent medium	7.6	6.7

another having a rough surface and clods at the surface and in the soil. We compared the results from the heterogeneous medium and that from an equivalent homogeneous medium. The latter corresponds to a medium having the same surface profile as the heterogeneous one but with a constant equivalent permittivity determined by the weighted sum of the two phases. Comparisons were drawn between the scatter diagrams and the evolution of energy computed at the center of the computation domain above the medium. The soil characteristics are summarized in Table II. In both cases, rather dry conditions were selected. With case 1, which is somewhat caricatural, a strong contrast between the fine earth and the clods was taken.

We simulated in case 2 a situation that was as close as possible to actual soil conditions. For this, we took profit of soil characterization, done after a tillage operation with a rotary arrow [32]. The clod-size distribution was determined, and the soil moisture and dry bulk density of both phases were measured. The dielectric constant was then derived using the Dobson soil-dielectric model [33], with the result of a moderate contrast ranging from 8.5 to 6 for the clod and the fine-earth phases, respectively.

The first case corresponds to a flat soil with clods imbedded below the surface (see case 1 in Table II). The soil structure simulated by the soil-geometry simulator is shown in Fig. 10, and the 2DSCAT simulation results are shown in Fig. 11.

In both cases, the main contribution to the scattering field is the specular reflection. The difference in the backscattered $|\mathbf{E}|^2$ from the homogeneous and heterogeneous media is equal to 1.9 dB. It is significantly higher than the model errors obtained with the test cases (Figs. 6–8) and shows that the clods below the surface have an impact in the scattering process. Differences in scattering fields become much stronger with angles

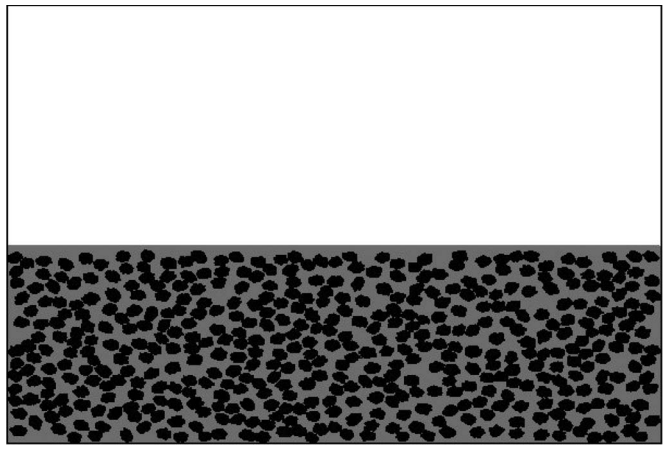

Fig. 10. Permittivity maps given by the soil-structure generator for case 1 (Table II—clods under a flat surface). Black color corresponds to clods having a higher permittivity.

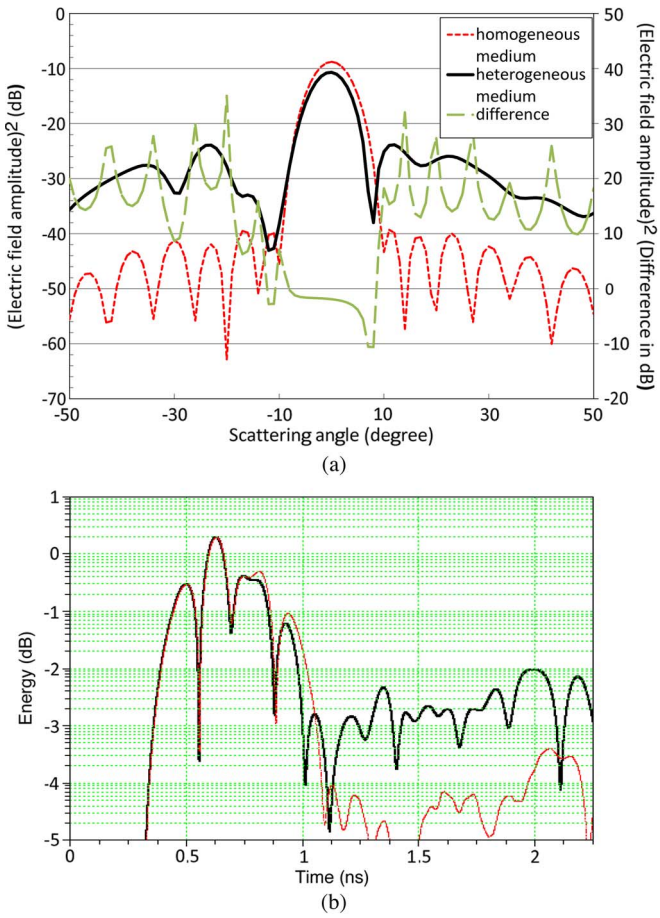

Fig. 11. Simulation results for case 1 (Table II—clods under a flat surface) with a vertical incident wave. (a) The scatter diagram and (b) the energy amplitude computed at the center of the computation domain above the soil.

larger than 5°, confirming the presence of volume scattering. The large difference in decibels, which is mainly due to the very low scattering from the homogeneous media, should be theoretically limited to the specular reflection. With the heterogeneous medium, the scattered field at incidence angle greater than 20° is comparable with that of a rough soil (Fig. 13)

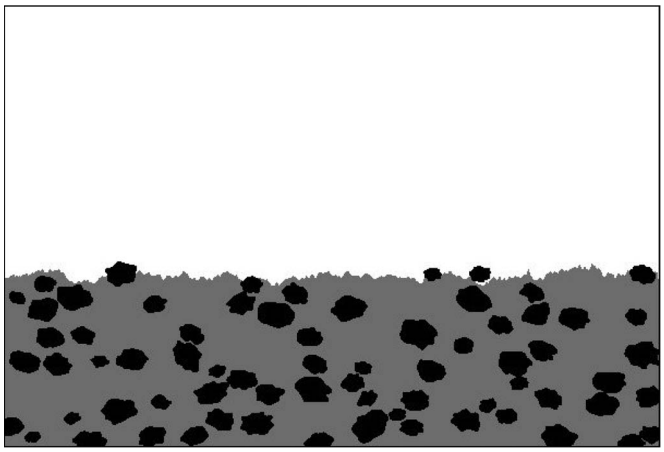

Fig. 12. Same as Fig. 10 for case 2 (Table II—rough soil with clods at the surface).

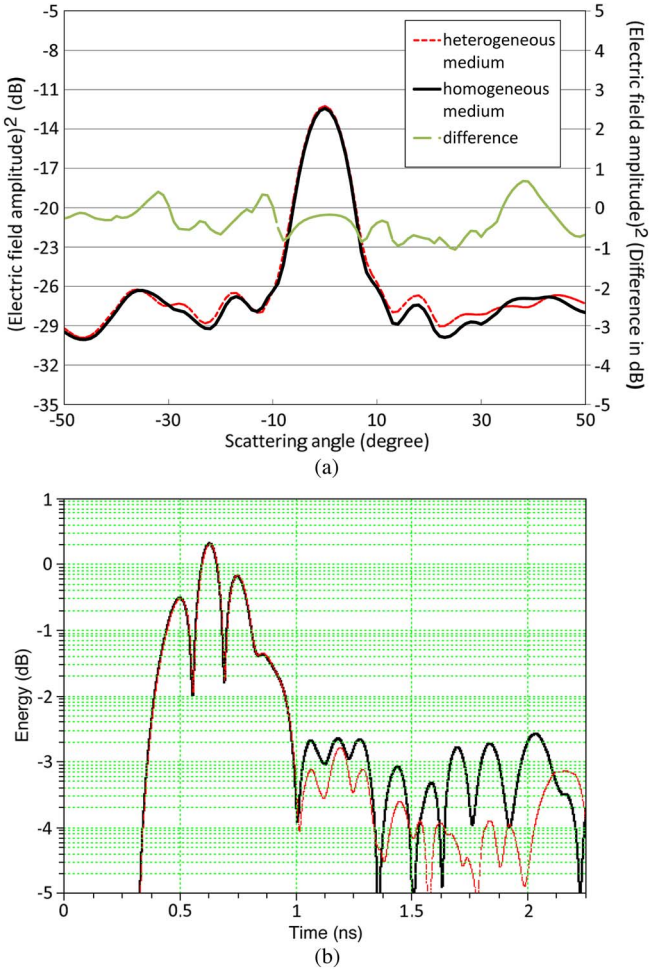

Fig. 13. Same as Fig. 11 with case 2 (Table II—rough soil with clods at the surface).

with an $|\mathbf{E}|^2$ ranging between -25 and -30 dB. The volume scattering also affects the temporal signal of the energy above the surface by maintaining a higher level of energy beyond 1 ns [Fig. 11(b)].

The second case corresponds to the rough surface (see Table II, case 2), with clods located both in the soil and at the soil surface. The generated soil geometry is shown in Fig. 12, and the results from the 2DSCAT are shown in Fig. 13.

As with the first case, the specular reflections from the homogeneous and heterogeneous cases are comparable. Surprisingly, the patterns of the diffusion diagram at higher scattering angles are very similar, showing that surface scattering dominates the scattering processes. The difference in $|\mathbf{E}|^2$ never exceeds 1 dB. This may be explained by the smaller number of clods (26% of the surface) used in this case compared with case 1 (51% of the surface). However, simulations made with a higher density of clods showed similar results. Again, the energy of the temporal signal persists longer in the case of the heterogeneous medium. This confirms that volume scattering occurred but did not significantly alter the angular patterns of the scattered electric field. Therefore, surface scattering is the dominant scattering process on rough surfaces, thus explaining the success of surface-scattering models. The contribution of the volume scattering remains lower than 1 dB, which falls within the range of errors made on the scattering fields due to roughness-characterization uncertainties [10]. This explains why the volume-scattering contribution is difficult to evaluate from experimental results. The case 2 results were obtained with a rather dry soil. In wetter conditions, we do not expect a stronger contribution of the volume scattering since the weaker wave penetration should enhance surface scattering.

To characterize the inner structure of soil, classical radar measurements based on the amplitude of the scattering field do not provide relevant information. Since clod size and surface roughness are correlated, an indirect evaluation of the clod size can be made by analyzing the surface-roughness patterns. The temporal signal seems to be the most interesting characteristic to analyze and separate the volume-scattering contribution, which requires recording of the temporal signals with an instrument such as a georadar. Another avenue would be the analysis of cross-polarization signatures.

VI. Conclusion

In this paper, we have presented the combination of a microwave-scattering model and a soil-geometry simulator, which offer an original simulator of 2-D EM scattering from soils. We have demonstrated its abilities to represent the microwave backscattering results on heterogeneous media composed of soil aggregates. This means that a 2-D representation, which strongly reduces the size of the numerical problem, is suitable to represent tilled soil as the copolarized scattering from heterogeneous media.

Analysis of the 2DSCAT model outputs shows the strong influence of surface scattering. In the studied cases, the volume scattering does not produce specific scattering angular patterns when a rough surface is present. However, a time-domain study of the scattering signal seems to be an interesting way to get volume information even with rough surfaces. The 2DSCAT model can be a useful tool to better define the significance of an equivalent permittivity by considering the soil structure and the vertical gradients. Another endeavor will be the development of

a 3-D version, which allows analysis of the influence of volume scattering on depolarization.

ACKNOWLEDGMENT

The authors would like to thank H. Tortel of the Fresnel Institut in France for his good advice and the implementation of the analytic formula for the infinite cylinder problem, and the National Computer Centre of Higher Education (C.I.N.E.S.) in France for the computational resources located at the SGI Origin supercalculator.

REFERENCES

[1] C. Durr and J.-N. Aubertot, "Emergence of seedlings of sugar beet (Beta vulgaris L.) as affected by the size, roughness and position of aggregates in the seedbed," *Plant Soil*, vol. 219, no. 1/2, pp. 211–220, Mar. 2000.

[2] H. Lu, T. Koike, H. Tsutsui, T. Graf, D. N. Kuria, H. Fujii, and M. Mourita, "A radiative transfer model for soil media with considering the volume effects of soil particles: Field observation and numerical simulation," in *Proc. IGARSS*, Denver, CO, 2006, pp. 1736–1739.

[3] G. G. Schaber, "SAR studies in the Yama Desert, Arizona: Sand penetration, geology and the detection of military ordnance debris," *Remote Sens. Environ.*, vol. 67, no. 3, pp. 320–347, Mar. 1999.

[4] E. Schanda, "On the contribution of volume scattering to the microwave backscattered signal from wet snow and wet soil," *Int. J. Remote Sens.*, vol. 8, no. 10, pp. 1489–1500, Oct. 1987.

[5] A. K. Fung, *Microwave Scattering and Emission Models and Their Applications*. Norwood, MA: Artech House, 1994.

[6] P. Xu and L. Tsang, "Bistatic scattering and emissivities of lossy dielectric surfaces with exponential correlation functions," *IEEE Trans. Geosci. Remote Sens.*, vol. 45, no. 1, pp. 62–72, Jan. 2007.

[7] A. Darawankul and J. T. Johnson, "Band-limited exponential correlation function for rough-surface scattering," *IEEE Trans. Geosci. Remote Sens.*, vol. 45, no. 5, pp. 1198–1206, May 2007.

[8] D. N. Kuria, T. Koike, H. Lu, H. Tsutsui, and T. Graf, "Field-supported verification and improvement of a passive microwave surface emission model for rough, bare, and wet soil surfaces by incorporating shadowing effects," *IEEE Trans. Geosci. Remote Sens.*, vol. 45, no. 5, pp. 1207–1216, May 2007.

[9] G. Macelloni, G. Nesti, P. Pampaloni, S. Sigismondi, D. Tarchi, and S. Lolli, "Experimental validation of surface scattering and emission models," *IEEE Trans. Geosci. Remote Sens.*, vol. 38, no. 1, pp. 459–469, Jan. 2000.

[10] H. Lievens, H. Vernieuwe, J. Alvarez-Mozos, B. De Baets, and N. E. C. Verhoest, "Error in radar-derived soil moisture due to roughness parameterization: An analysis based on synthetical surface profiles," *Sensors*, vol. 9, no. 2, pp. 1067–1093, Feb. 2009.

[11] N. E. C. Verhoest, H. Lievens, W. Wagner, J. Alvarez-Mozos, S. Moran, and F. Mattia, "On the soil roughness parameterization problem in soil moisture retrieval of bare surfaces from synthetic aperture radar," *Sensors*, vol. 8, no. 7, pp. 4213–4248, 2008.

[12] M. Zribi, O. Taconet, S. Le Hégarat-Mascle, D. Vidal-Madjar, C. Emblanch, C. Loumagne, and M. Normand, "Backscattering behavior and simulation comparison over bare soils using SIR-C/X-SAR and ERASME 1994 data over Orgeval," *Remote Sens. Environ.*, vol. 59, no. 2, pp. 256–266, Feb. 1997.

[13] J. B. Boisvert, Q. H. J. Gwyn, A. Chanzy, D. J. Major, B. Brisco, and R. J. Brown, "Effect of surface soil moisture gradients on modelling radar backscattering from bare fields," *Int. J. Remote Sens.*, vol. 18, no. 1, pp. 153–170, Jan. 1997.

[14] A. Le Morvan, M. Zribi, N. Baghdadi, and A. Chanzy, "Soil moisture profile effect on radar signal measurement," *Sensors*, vol. 8, no. 1, pp. 256–270, 2008.

[15] J.-P. Wigneron, L. Laguerre, and Y. H. Kerr, "A simple parameterization of the L-band microwave emission from rough agricultural soils," *IEEE Trans. Geosci. Remote Sens.*, vol. 39, no. 8, pp. 1697–1707, Aug. 2001.

[16] M.-J. Escorihuela, A. Chanzy, J.-P. Wigneron, and Y. H. Kerr, "Effective soil moisture depth of L-band radiometry: A case study," *Remote Sens. Environ.*, vol. 114, no. 5, pp. 995–1001, May 2010.

[17] K. Schneeberger, M. Schwank, C. Stamm, P. De Rosnay, C. Mätzler, and H. Flüher, "Topsoil structure influencing soil water retrieval by microwave radiometry," *Vadoze Zone J.*, vol. 3, no. 4, pp. 1169–1179, 2004.

[18] F. M. Kahnert, "Numerical methods in electromagnetic scattering theory," *J. Quant. Spectrosc. Radiat. Transf.*, vol. 79/80, no. 1, pp. 775–824, 2003.

[19] J. F. Lee, R. Lee, and A. Cangellaris, "Time-domain finite element methods," *IEEE Trans. Antennas Propag.*, vol. 45, no. 3, pp. 430–442, Mar. 1997.

[20] E. Bachelier, "Modélisation électromagnétique des effets de diffusion de durface et de volume des sols par la méthode des différences finies," Ph.D. dissertation, Ecole Nationale Supérieure de l'Aéronautique et de l'Espace, Toulouse, France, 1999.

[21] C. Durr, J.-N. Aubertot, G. Richard, P. Dubrulle, Y. Duval, and J. Boiffin, "Simple: A model for simulation of plant emergence predicting the effects of soil tillage and sowing operations," *Soil Sci. Soc. Amer. J.*, vol. 65, no. 2, pp. 414–423, Mar./Apr. 2001.

[22] A. Chambarel and E. Ferry, "Finite element formulation for Maxwell's equations with space dependent electric properties," *Revue Européenne des éléments finis*, vol. 9, no. 8, pp. 941–967, 2000.

[23] H. Bolvin, A. Chambarel, and A. Chanzy, "Three-dimensional numerical modelling of a capacitance probe: Application to measurement interpretation," *Soil Sci. Soc. Amer. J.*, vol. 68, no. 2, pp. 440–446, Mar./Apr. 2004.

[24] J.-P. Berenger, "A perfectly matched layer for the absorption of electromagnetic-waves," *J. Comput. Phys.*, vol. 114, no. 2, pp. 941–967, Oct. 1994.

[25] A. Taflove and S. C. Hagness, *Computational Electrodynamics: The Finite Time-Domain Method*, 3rd ed. Boston, MA:Artech House, 2005.

[26] D. Katz, E. T. Thiele, and A. Taflove, "Validation and extension to three dimension of the Berenger PML absorbing condition for FD-TD meshes," *IEEE Microw. Guided Wave Lett.*, vol. 4, no. 8, pp. 268–270, Aug. 1994.

[27] S. J. Orfanadis, Electromagnetic Waves and Antennas, 2008. [Online]. Available: http://www.ece.rutgers.edu/~orfanidi/ewa

[28] J. A. Stratton and L. J. Chu, "Diffraction theory of electromagnetic wave," *Phys Rev.*, vol. 56, no. 1, pp. 99–107, Jul. 1939.

[29] C.-T. Tai, "Kirchhoff theory: Scalar, vector or dyadic," *IEEE Trans. Antennas Propag.*, vol. AP-20, no. 1, pp. 114–115, Jan. 1972.

[30] J. A. Kong, *Electromagnetic Wave Theory*. Cambridge, MA: EMW Publishing, 2005.

[31] R. Rouveure, "Caractérisation de l'état de surface du sol à courte distance par des techniques mico-ondes—Application à la mesure de la rugosité d'un sol agricole," Ph.D dissertation, Sciences pour l'ingénieur, Université Blaise Pascal, Clermont Ferrand II, Clermont-Ferrand, France, 2001.

[32] G. Richard, R. Rouveure, A. Chanzy, P. Faure, M. Chanet, A. Marionneau, P. Régnier, and Y. Duval, "Continuous monitoring of agricultural soil physical conditions using proximal sensors for soil tillage management," in *Proximal Soil Sensing*, R. A. Viscarra Rossel, A. McBratney, and B. Minasny, Eds. Dordrecht, The Netherlands: Springer-Verlag, 2010, ser. Progress in Soil Science, to be published.

[33] M. C. Dobson, F. Kouyate, F. T. Ulaby, M. T. Hallikainen, and M. A. El Rayes, "Microwave dielectric behaviour of wet soil—Part II: Dielectric mixing models," *IEEE Trans. Geosci. Remote Sens.*, vol. GRS-23, no. 1, pp. 51–61, Jan. 1985.

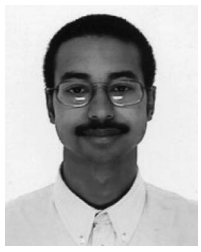

Charles Onier was born in 1980. He received the M.S. degree in electrical engineering from the Polytech'Nice-Sophia School, Nice, France, in 2003, the M.S. degree in propagation, telecommunication, and remote sensing from the University of Nice-Sophia Antipolis, Nice, France, in 2003, and the Ph.D. degree in earth sciences from the University of Avignon and Vaucluse's land, France.

Since 2008, he has been an Assistant Professor with the University of Nice-Sophia Antipolis, attached to the Electronics, Antennas and Telecommunications Laboratory (LEAT), a joint research laboratory supported by CNRS and the University of Nice-Sophia Antipolis. His current research interests include georadar signal processing from UWB, multistatic, multipolarization, wide-offset microwave data, and ground imaging.

André Chanzy received the Ph.D. degree in physics of the environment from the Institut National Agronomique Paris-Grignon, Paris, France, in 1991.

He has been with the Soil Science Laboratory, Avignon INRA Research Center, Avignon, France, since 1987. He was the Head of the Joint research Unit Climate Soil and Environment of the INRA Institute and Avignon University from 1999 to 2007. He is currently with the joint INRA/Avignon University laboratory "Environnement Méditerranéen et Modélisation des AgroHydrosystèmes" and currently leads the "Adaptation to Global Change" program of the Avignon INRA center. His scientific fields of interest are soil water-flow modeling and the application of remote sensing (active and passive), and *in situ* observations to infer hydrological fluxes.

André Chambarel was born in France, in 1944. He received the Ph.D. degree from the University of Avignon and Vaucluse's land, France, in 1975.

From 1967 to 1975, he was an Assistant Professor with the University of Avignon. From 1975 to 1980, he was with the University of Technology of Compiègne, France. From 1980 to 1997, he was with the University of Aix-Marseille I, Marseille France. Since 1997, he has been a Professor with the University of Avignon, attached to the "Modelling Agricultural and Hydrological Systems in the Mediterranean Environment" Laboratory, jointly supported by INRA and the University of Avignon. His current research interests include the study of complex porous media, the study of the response of instruments measuring the electrical properties of soil, the propagation of electromagnetic waves, and of mechanical waves in porous media, having designed a development platform by the finite-element method.

Raphaël Rouveure was born in 1966. He received the B.S. degree in electrical engineering degree from the Polytech' Clermont School of Engineering, Clermont-Ferrand, France, in 1990 and the Ph.D. degree in sciences for engineering from the University of Clermont 2, Clermont-Ferrand, in 2001.

He is associated with the Ecotechnology and Agrosystem Department, Institute for Agricultural and Environmental Engineering Research (CEMAGREF), France. His current research activities are in the development of new sensors for environmental application. His work deals with signal processing and technology in the microwave domain.

Myriam Chanet was born in 1963. She received the electrical engineering degree from the Polytech' Clermont School of Engineering, Clermont-Ferrand, France, in 1987 and the Ph.D. degree in control engineering from the Centrale Lyon School, Lyon, France, in 1996.

She is with the Ecotechnology and Agrosystem Department, Institute for Agricultural and Environmental Engineering Research (CEMAGREF), France. Her current research activities are in the development of new device for environmental application.

Hervé Bolvin was born in 1947. He received the M.S. degree in fundamental physics and the Ph.D. degree in molecular spectroscopy from the University of Lille, Villeneuve d'Ascq, France, in 1971 and 1988, respectively, and the habilitation from the University of Avignon and Vaucluse's land, France, in 2004.

From 1974 to 1984, he was an Assistant Professor in cultural cooperation in Morocco. From 1984 to 2003 he was attached to the "Physics of Lasers, Atoms and Molecules" Laboratory (PhLAM), a joint research laboratory supported by CNRS and the University of Lille. Since 2003, he was with the "Modeling Agricultural and Hydrological Systems in the Mediterranean Environment" Laboratory, jointly supported by INRA and the University of Avignon. His current research interests include modeling phenomena of electromagnetic-wave propagation in soil taking into account the dielectric loss.